JOURNAL OF GUIDANCE, CONTROL, AND DYNAMICS
Vol. 27, No. 1, January–February 2004

Toward a Stellar Gyroscope for Spacecraft Attitude Determination

Carl Christian Liebe,* Konstantin Gromov,† and David Matthew Meller†
Jet Propulsion Laboratory, California Institute of Technology, Pasadena, California 91109-8099

A stellar gyroscope is a star tracker that can operate at high slew rates and high update rates. Stellar gyroscopes can potentially eliminate the need for conventional inertial gyros onboard a spacecraft and will eventually revolutionize attitude determination systems on all spacecraft. A conceptual design of a stellar gyroscope will be presented along with simulations of the stellar gyroscope performance. The simulations show that it is feasible to make spacecraft attitude determination relying exclusively on stellar gyroscopes. It is projected that the stellar gyroscope will be able to determine slew rates up to 420 deg/s and will be able to determine the absolute attitude at slew rates up to 50 deg/s.

Introduction

MOST spacecraft missions use a star tracker for three-axis attitude determination. Fundamentally a star tracker is an electronic camera connected to a computer. Using a sensed image of a portion of the sky, stars can be located and identified. A spacecraft must be stabilized to some extent before a traditional star tracker can begin to determine the attitude (typically a few degrees/second). Therefore, a gyroscope typically compliments the star tracker. The gyroscope is used for the initial stabilization of the spacecraft and for high-frequency attitude updates. This paper proposes a very fast and wide field-of-view (FOV) star tracker to operate at high update and slew rates. Stellar gyroscopes eliminate the need for a gyroscope (and other attitude determination sensors) on a spacecraft. A gyroless spacecraft will have significantly lower power consumption, mass, and complexity compared to spacecraft utilizing conventional attitude determination systems.

Star trackers have been commercially available for more than a decade. All current commercial star trackers utilize charge-coupled-device (CCD) chips. The primary reason for this is that CCD chips have low noise and are widely available. Star trackers typically have a mass of $\sim$3 kg and a power consumption of $\sim$10 W. They typically have an update rate of $<$5 Hz and can operate up to a slew rate of a few degrees/second (Refs. 1–6).

The combination of inertial and celestial sensors used in current spacecraft designs is typically massive (3 to 20 kg), physically large, and consumes large amounts of power (15 to 200 W) (Ref. 7). Current spacecraft utilize discrete sensor-system components to gather measurement data to a central processor that uses onboard algorithms to provide attitude information. This approach leads to many hardware and software interface issues during integration, test, and in-flight operations. Stellar gyroscopes will provide all of the information traditionally gathered using other attitude sensors. The elimination of a gyroscope, a traditional CCD-based star tracker, and a sun sensor on a spacecraft will reduce the mass and power consumption of the attitude determination and control system (ADCS) by one to two orders of magnitude. Also, the complexity of the ADCS will be greatly reduced.

A few attempts have been made to make a CCD-based star tracker operate at high slew rates. In these cases the rotation axis of the spacecraft was known a priori, and the star tracker was pointed orthogonal to the rotation axis. When the image was read out, it was shifted precisely opposite the spacecraft rotation, so that the collecting charge remained fixed in inertial space. This technique is called time-delayed integration. However, it only works for rotations about an orthogonal spin axis and cannot be used to detumble a spacecraft.

Recently, two different developments of active-pixel-sensor (APS)-based star trackers have been initiated. These star trackers can measure attitude rates at high slew rates and high update rates. The two star trackers include conventional or micro-electromechanical-based gyroscopes and do not estimate the slew rates based on optical measurements.[8,*]

Never before have star trackers been designed to operate at the update rates or the slew rates of a gyroscope. A critical spin rate is $\sim$70 rpm, which is a typical rate for deployment from a launch vehicle. If the stellar gyroscope cannot operate at this rate, a gyroscope is still needed for initial stabilization and fault scenarios. In recent years, technology (processor speed and APS chips) has reached a stage where it is becoming feasible to substitute a gyroscope with a star tracker. This opens up the possibility of a complete paradigm shift in attitude determination system design based exclusively on stellar gyroscopes.

A stellar gyroscope also has rocket applications. When the vehicle has reached orbit, it must acquire its attitude, while spinning at a high rate. A stellar gyroscope mounted with the boresight along the spin axis can perform this attitude acquisition.

The stellar gyroscope also has limitations compared to a conventional inertial gyro. This is because the stellar gyroscope must constantly image stars to operate. On the surface of any planet with an appreciable atmosphere (e.g., Earth or Mars), no stars will be visible during the day because of the skylight, and the stellar gyroscope cannot operate. If the stellar gyroscope is used on a satellite in low Earth orbit, it will not be able to operate while looking toward the Earth, moon, sun, or with stray light in the FOV. Utilizing more than one stellar gyroscope on a spacecraft pointing in different directions can mitigate most of these problems.

Stellar Gyroscope Operation

When a fast and wide FOV camera is operated on a three-axis-stabilized spacecraft with an integration time of 50 ms, for example, it will detect many stars. A simulated image from a camera mounted on a three-axis-stabilized spacecraft is shown in Fig. 1. In this specific camera configuration and orientation, stars as faint as $M_V \sim 4.3$ are detected by visual inspection of the image. (Silicon-based image detectors tend to be more sensitive in the red/near IR than the

Received 20 September 2002; revision received 17 February 2003; accepted for publication 20 August 2003.

*Senior Member of Technical Staff, 4800 Oak Grove Drive.
†Member of Technical Staff, 4800 Oak Grove Drive.

*Data available online at http://www.jungfrau.tamu.edu/~html/StarNav/home.html [cited 1 August 2003].

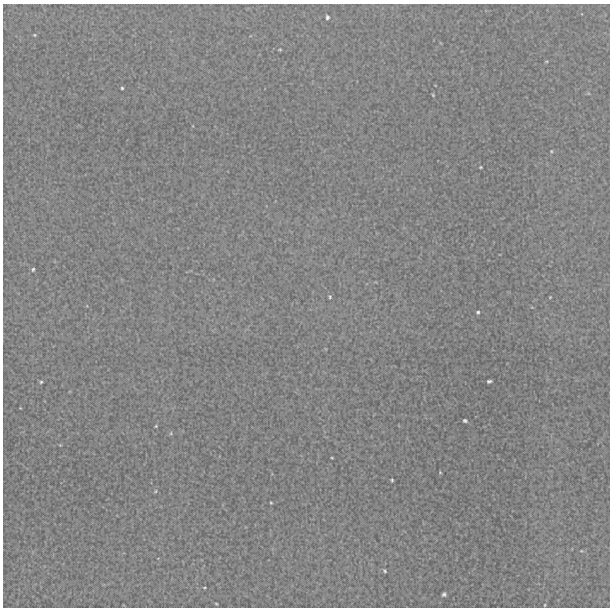

Fig. 1 Simulated star image ($\delta = 37$ deg, $\alpha = 191$ deg) contrast enhanced. The Big Dipper is observed in the lower right part of the image. The camera was three-axis stabilized during the exposure. The FOV is 56 deg, the exposure time is 50 ms, and the lens aperture is 8 mm. The read noise is 30 photoelectrons, and the dark current is 70 pA/cm^2. The detector consists of 356 $\times$ 356 pixels, each of 18 $\times$ 18 microns. The optical focal length is 6 mm. A camera sensitivity of 13,000 photoelectrons per second per mm^2 lens aperture for a M_V 0 star was assumed.

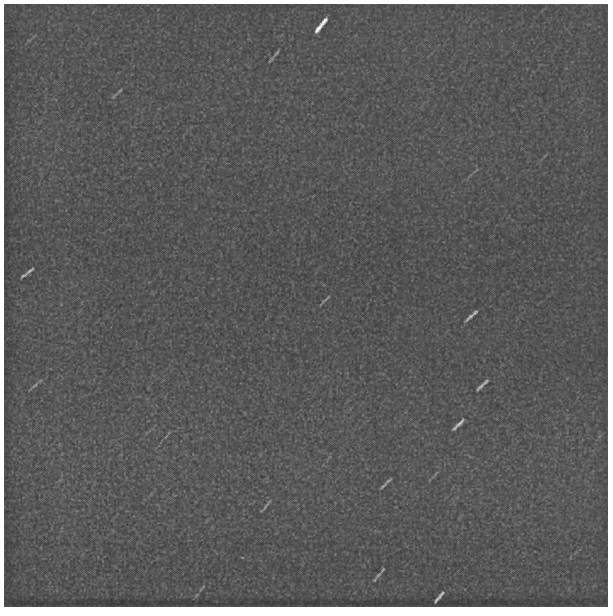

Fig. 2 Simulated star image ($\delta = 37$ deg, $\alpha = 191$ deg) contrast enhanced. The camera was slewing 28 deg/s cross boresight. The camera configuration is similar to the configuration in Fig. 1.

human eye. Therefore, low-surface-temperature stars will be perceived brighter than other stars. In this paper visual magnitude M_V is used with the underlying assumption that all stars have a surface temperature of 5800 K.) The star identification algorithms recognize the constellation and report the absolute star tracker orientation to the spacecraft. For details on star tracker operation, see Ref. 9.

In Fig. 2 another scenario is simulated. The spacecraft is slewing at a low angular rate (cross boresight) of 28 deg/s. It is observed that the stars are smeared out over several pixels. Because of this, the signal-to-noise (S/N) ratio decreases, and faint stars are not detected anymore. In this specific configuration and orientation the detection

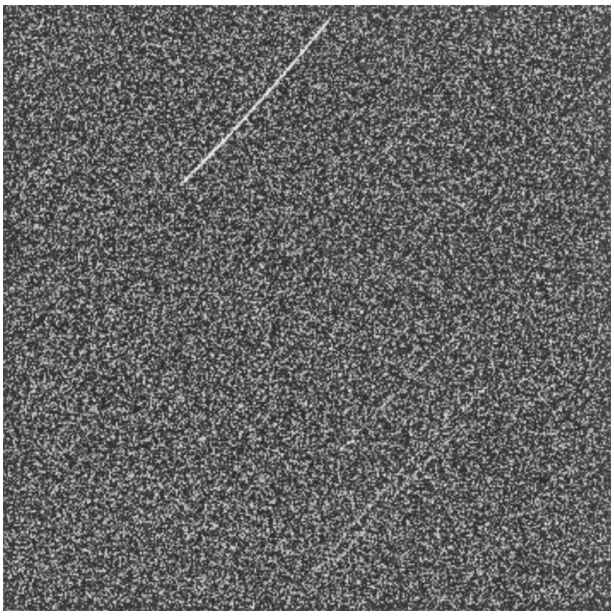

Fig. 3 Simulated star image ($\delta = 37$ deg, $\alpha = 191$ deg) contrast enhanced. The camera was slewing 420 deg/s in a cross-boresight axis. The camera configuration is similar to the configuration in Fig. 1.

threshold has decreased to $M_V \sim 3.6$ based on visual inspection of the image. However, the star tracker algorithms are still able to calculate the absolute attitude.

In Fig. 3 yet another scenario is discussed. The spacecraft is now slewing at a high angular rate of 420 deg/s (cross boresight). It is observed that the stars are smeared out over many pixels. Because of this, the S/N is decreased further, and only a few very bright stars are detected by visual inspection of the image. (The bright star is M_V 0.0, and the dim star streak in the lower right corner is M_V 1.9.) It is no longer possible for the star tracker algorithm (or the human brain, for that matter) to recognize the star constellation and determine the absolute attitude. However, it is possible to determine the length and the shape of the star streaks. This provides information about the spin rate and the spin axis, that is, information similar to that which a traditional inertial gyroscope can provide.

In the image shown in Fig. 3 it is not possible to determine the polarity of the spin. That is, did the stars move from the southwest corner toward the northeast corner, or vice versa? It is impossible to derive this information based on a single image. However, it is possible to work around the problem. Two different images can be acquired in fast sequence, and the spin direction can then be determined.

In the scenarios shown in Figs. 2 and 3, the slew was primarily in a cross-boresight axis. The rotation axis can also be primarily in the boresight axis (or any combination). Rotation about the boresight axis results in shorter star streaks compared to rotation about a cross-boresight axis. In particular, stars close to the rotation axis will generate short star streaks. Figure 4 shows the same scenario as in Fig. 3. However, the rotation is now primarily in the boresight axis. It is observed that dimmer stars are detected and the star streaks are shorter. The bright star close to the center is M_V 2.9. Slew rates around the cross-boresight axis present more difficulty (in terms of S/N) for the stellar gyroscope than slew rates around the boresight axis.

Based on the discussion in this section, it becomes clear that a stellar gyroscope must operate in one of two different modes: 1) absolute attitude mode, where the stellar gyroscope calculates the absolute attitude relative to the celestial sphere similar to a conventional star tracker; and 2) relative attitude mode, where the stellar gyroscope calculates the change in attitude during the exposure similar to an inertial gyroscope. These two modes will be discussed in greater detail later in this paper.

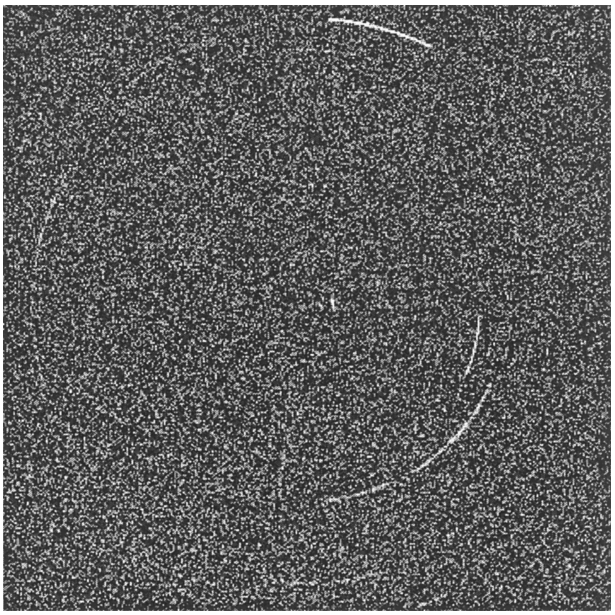

Fig. 4 Simulated star image ($\delta = 37$ deg, $\alpha = 191$ deg) contrast enhanced. The camera was slewing 420 deg/s around the boresight axis. The camera configuration is similar to the configuration in Fig. 1.

Conceptual Design of the Stellar Gyroscope

The single most critical property for constructing a successful stellar gyroscope is to detect as many stars as possible. The five factors that determine the number of detected stars are as follows:

1) Field of view is the first factor. The wider the field of view, the more bright stars will be in the field of view. There are three disadvantages of utilizing a wide FOV:

a) The star tracker will not be able to operate with the sun in the FOV; therefore, wide FOV means a large exclusion angle from the sun.

b) It can be difficult to mount the star tracker on the spacecraft and have a wide unobstructed FOV.

c) The accuracy of the stellar gyroscope operating as a star tracker will be less accurate in cross-boresight accuracy.

2) Optical collecting power of the system is the next factor. The more optical collecting power inherent in the system, the more sensitive the system becomes, and the more stars will be detected. This means that the aperture should be large. The ratio of the focal length to the aperture diameter is the f number (f/#) of the lens. The theoretical limit is 0.5, but very few lenses have been built with f/# < 0.75. [An example of a flight qualified fast lens has f/# $= 0.69$ (Ref. 2).]

3) The third factor is effective exposure time. The effective exposure time is the time that a star will illuminate a specific pixel when the star slews across the focal plane. As an example, a stellar gyroscope has a FOV of 50 deg, and the focal plane consists of 512×512 pixels. The slew rate is 170 deg/s. The effective exposure time is therefore (50 deg/512 pixels)/170 deg/s $= 0.57$ ms/pixel. Note that the exposure time of the focal plane is not related to the effective exposure time and only determines the length of the star streak. Therefore, at high rates it is better to have fewer, larger pixels than many small pixels. Unfortunately, large pixels can be a two-edged sword because dark current is proportional to pixel area, and read noise increases with pixel size.

4) Image detector technology is the fourth factor. It is important to have an image detector with as high quantum efficiency and as low noise as possible.

5) Point spread function is the final factor. The point-spread function of the lens must be as small as possible to increase the S/N ratio. This is different from a conventional star tracker, where the optics is typically defocused slightly to increase the accuracy.[9]

It is important to have a wide FOV for another reason: When the spin axis is at a large angle from the boresight (i.e., close to cross boresight), the star streaks become nearly linear, with little curvature. When the images are noisy and only a small segment of the star streak is recorded, it is very difficult to accurately determine the spin axis. A wider FOV will allow a larger fraction of the star streak to be included in the image, and a more accurate determination of the spin axis.

Table 1 APS detector characteristics

Characteristics	Value
Read noise	30 photoelectrons
Dark current	70 pA/cm^2
Format	356×356 pixels
Pixel pitch	18 microns
A/D bits	10
Pixel read frequency	10 MHz

In this paper a conceptual design of a stellar gyroscope is presented. The two key elements on which this paper has focused are the optics and the focal plane. The focal plane data that must be processed also represent a significant challenge. However, the processing architecture of a stellar gyroscope is not addressed in this paper.

As part of the conceptual design, an APS chip is proposed. Traditionally, CCD chips have been utilized for star trackers because of their wide availability and low noise. However, APS chips are reaching a stage where they can compete with CCD chips with respect to these criteria.[10] With an APS chip it is possible to read out small windows on the focal plane corresponding to star locations at high update rates (>100 Hz). This ability would be difficult to match with a CCD chip. Also, all control circuitry and A/D conversion can be placed directly on the image detector die. The characteristics shown in Table 1 were chosen for the APS detector in this study. These values represent the state of the art in APS design.[11,*,†,‡]

The read noise of the APS chip used in this study is low when compared to commercially available APS detectors, which typically range from 40 to 80 photoelectrons. The low read noise of 30 photoelectrons is feasible if a special APS chip were designed for this application. This would require the full pixel well to be reduced to approximately 25% of normal and to utilize correlated double sampling. (Correlated double sampling means to read each pixel twice: in the beginning of the exposure and second at the end of the exposure. These values are then subtracted.) There are no physical laws prohibiting a read noise of 30 photoelectrons. Commercial CCD cameras regularly achieve a read noise of less than 20 photoelectrons.[§]

As stated earlier, it is desired to have as wide and fast optics as possible. Commercially, one of the widest and fastest lenses available is aspherical with a focal length of 6 mm and f/0.75.[¶] For this study, a lens with these parameters and a Gaussian point spread function (PSF) of 0.5 pixels was chosen. [A PSF of much smaller than 0.5 pixels will result in a sharp decline in the accuracy because of the sampling theorem (see Ref. 12, Fig. 14).] It has previously been documented that it is possible to design this type of instrument with less than 50 g of mass (not including the processing electronics).[13]

The simulation assumes that optical distortion can be removed by calibration, that no stray light is present, and that the readout noise is linear. A significant effort would be required to actually achieve this.

Stellar Gyroscope in Absolute Attitude Determination Mode

Conventional star trackers perform star identification (ID) and calculate a quaternion representing the rotation from inertial space

*Data available online at http://www.photobit.com/Products/Product_Matrix/product_matrix.htm [cited 6 March 2002].

†Data available online at http://e-www.motorola.com/brdata/PDFDB/docs/MCM20014.pdf [cited 6 March 2002].

‡Data available online at http://www.fillfactory.com/htm/cmos/htm/star250/star250.htm [cited 6 March 2002].

§Data available online at http://www.sbig.com/sbwhtmls/online.htm [cited 29 April 2002].

¶Data available online at http://www.panasonic.co.uk/nw/products/product.asp?c-WVLA608 [cited 6 March 2002].

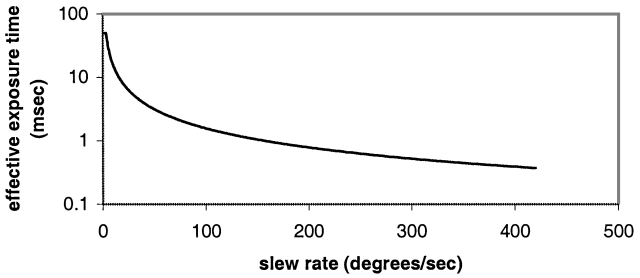

Fig. 5 Effective exposure time vs the cross-boresight slew rate for the stellar gyroscope.

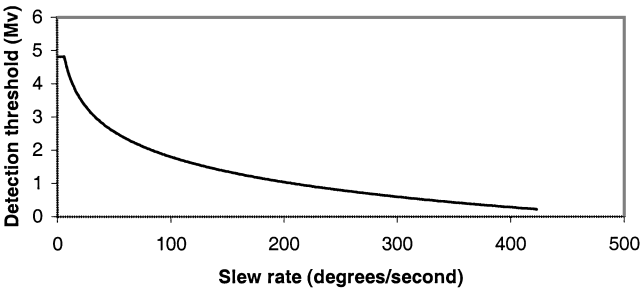

Fig. 6 Stellar detection threshold for the stellar gyroscope.

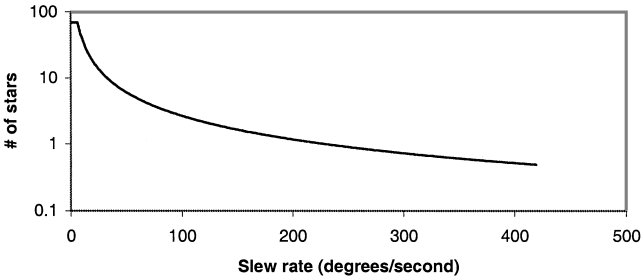

Fig. 7 Average number of stars in the FOV as a function of the cross-boresight slew rate.

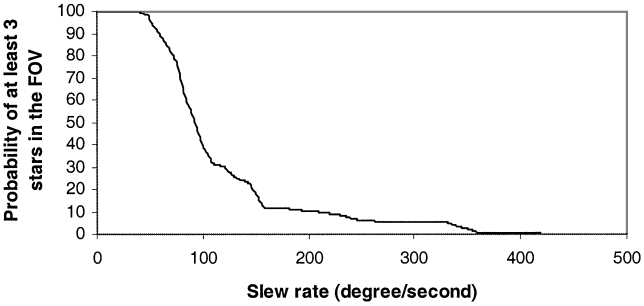

Fig. 8 Probability of having at least three detectable stars in the FOV.

to a star tracker-fixed coordinate system based on stars in the FOV. Theoretically, at least two stars must be identified in the FOV in order to calculate the quaternion. Typically, star trackers use a larger number of stars (4–50) (Refs. 14–18) to perform star ID. However, the FOV is narrower on conventional star trackers, and many more stars are involved in the star identification process.

The detection threshold and the number of detected stars will be discussed in this section. The first step is to determine the effective exposure time of a star, that is, the duration of time for which the light from a star illuminates a single pixel on the focal plane. In the conceptual stellar gyroscope design the FOV is 56 deg, and the APS detector consists of 356×356 pixels. Therefore, each pixel has an angular extent of 0.157 deg. The effective exposure time is shown as a function of the cross-boresight slew rate in Fig. 5. It is observed that the effective exposure time decreases rapidly as the slew rate increases. If the spin axis is close to the boresight, the effective exposure time will not decrease so rapidly.

The absolute sensitivity of an APS image detector is typically 13,000 photoelectrons/s/mm^2 for a M_V 0 star.[12,19] The chosen aperture of the stellar gyroscope optics is 8 mm, giving a front aperture area of 50.3 mm^2. Given an exposure time of 50 ms, an M_V 0 star will generate ~33,000 photoelectrons with the chosen aperture. At a slew rate of 100 deg/s, the length of the star streak is approximately 32 pixels. Depending on the point spread function, the charge from the star is spread over ~64 pixels. This means that a M_V 0 star will deposit, on average, ~516 photoelectrons in each pixel of the star streak. The read noise is 30 photoelectrons, and the dark current is assumed to be 70 pA/cm^2. The area of a pixel is $18 \times 18\ \mu\text{m} = 324\ \mu\text{m}^2$. The dark current is therefore $2.27 \cdot 10^{-16}$A. One electron has a charge of $1.602 \cdot 10^{-19}$C. The dark current is therefore 1418 photoelectrons/second. At 50 ms, the dark current is 71 photoelectrons, and the dark current noise will be sqrt (71) = 8.4 photoelectrons. The dark current nonuniformity is typically large, ~30%, but it can be mapped out. The rss of both the read noise and the dark current noise is ~32 photoelectrons. It is assumed that a star can be detected with a S/N ratio as small as 3. Under normal circumstances this would not be sufficient to detect a signal in a single pixel. In this specific case, however, a star streak consists of a large cluster of pixels above the background. Finally, we must account for the photon noise. The following equation is used because the photon noise must be combined with the rss of the read noise and dark current noise:

$$s = 3 \cdot \sqrt{32^2 + \sqrt{s^2}} \Rightarrow s = 100.6 \tag{1}$$

This means that a signal of 100.6 photoelectrons can be detected. It was previously established that a M_V 0 star generates 516 photoelectrons per pixel. The M_V detection threshold is therefore

$$\text{Detection threshold} = \frac{\ell_n(516/100)}{\ell_n 2.5} = 1.8 \tag{2}$$

The preceding detection threshold calculation was performed for many different slew rates. The result of the simulation is shown in Fig. 6.

A 56-deg, round FOV is assumed, which covers ~5.8% of the firmament. It is possible to calculate the number of stars corresponding to a given detection threshold: $N = 6.58 \cdot e^{1.08 \cdot M}$ (Ref. 12). The graph shown in Fig. 6 is transformed into the average number of stars detected in the FOV as a function of the slew rate. This is shown in Fig. 7.

At least two identified stars are required to calculate the absolute attitude of the stellar gyroscope. However, it can be difficult to discriminate two stars if they are identical in brightness. Therefore, it is assumed in this paper that it is possible to calculate the absolute attitude if three stars are identified. A simulation has been performed to estimate the percentage of cases where three or more detectable stars are present in the FOV as a function of the slew rate. The result is shown in Fig. 8. It is observed that at slew rates up to ~50 deg/s, at least three detectable stars are guaranteed to be in the FOV. This leads to the conclusion that the stellar gyroscope will always be able to establish the absolute attitude at slew rates up to 50 deg/s. At greater rates, for example, 200 deg/s, the probability of having at least three detectable stars in the FOV decreases to ~10%.

Stellar Gyroscope Accuracy in Absolute Attitude Determination Mode

The cross-boresight accuracy of the stellar gyroscope depends on the number of stars detected. Typically, it is possible to determine the position of a star with an accuracy of a small fraction of a pixel. The accuracy depends on a number of factors, such as the brightness of the star, pixel homogeneity, read noise, dark current, etc.[12,20] It is conservatively assumed that it is possible to determine the centroid of a star with an average accuracy of 0.3 pixels. Each pixel has an angular extent of 0.16 deg. Assuming that 10 stars are being tracked simultaneously, the star tracker accuracy is then (0.16 deg · 0.3)/sqrt(10) = 55 arcsec. Conventional star trackers typically exhibit better accuracy; however, most spacecraft missions do not require the high accuracy of a conventional star tracker.

When the stellar gyroscope is slewing at a rate of up to 50 deg/s, it will still be able to determine the absolute attitude. However, the stars are smeared out in streaks, and so it is conservatively assumed that it is only possible to determine the centroid of a star to an accuracy of 1 pixel. Detecting three stars will therefore result in an accuracy of 0.16 deg/sqrt (3) = 0.09 deg.

Stellar Gyroscope Update Rate in Absolute Attitude Determination Mode

The preceding figures in this paper have shown images as full frame images. However, only small areas of these images (where stars appear) contain useful information. If the stellar gyroscope is three-axis stabilized or slewing at a moderate rate, the stars will appear at almost the same position in the next image as in the preceding image. Therefore, it is not necessary to read out the entire image. It is only necessary to read out the pixels in a small window where stars are known to be located. APS chips can be designed to randomly access pixels. It is typically possible to read pixels from an APS chip with a speed of 10 MHz. Suppose a star tracker is tracking five stars and a region of 8×8 pixels around a star is read out at every update. This is a total of 320 pixels, or 32 μs. Assume that the exposure time is decreased to 5 ms in this tracking mode. The exposure time plus read time will result in an update frequency of 198 Hz. Suppose that it is acceptable for the position of a star to shift up to 2 pixels at each update, while still permitting the window position to be updated (this is reasonable with 8×8 pixel windows). It is then possible to allow the stellar gyroscope to move 396 pixels per second or 62 deg/s. In absolute attitude mode, the stellar gyroscope will therefore acquire a full frame, and in successive frames it will read only small windows where previous detected stars are known to be located.

Algorithms Used for Slew Rate and Axis Determination

When the stellar gyroscope is slewing at high rates ($\sim$100 deg/s), it is no longer possible to detect more than two stars and therefore is not possible to determine the absolute attitude. However, it is likely that one or two stars are still visible in the FOV, as shown in Figs. 3 and 4. These stars will form a star streak. It will be shown in this section that this star streak contains information similar to what a conventional gyroscope can provide.

Initially, the probability of detecting at least one star in the FOV is shown in Fig. 9. The simulation shows that at spin rates up to $\sim$90 deg/s at least one star will always be detected in the FOV, and the stellar gyroscope will operate over 100% of the sky. When the stellar gyroscope is rotating faster than $\sim$90 deg/s, it will not always detect a star in the FOV. As an example, at 420-deg/s spin rate the probability of detecting a star is only $\sim$50%. This means that the stellar gyroscope will only provide relative attitude data 50% of the time. However, at this fast slew rate no attitude initialization has been possible, and therefore it is not necessary to integrate the attitude estimate based on the gyros. The raw spin rates are sufficient to despin/detumble the spacecraft, and 100% sky coverage is not essential.

It was described earlier that a stellar gyroscope exposes for a relatively short time, for example, 50 ms. During this short time, the stellar gyroscope will rotate around a combination of three orthogonal axes caused by the spacecraft rotation. A conventional inertial gyroscope outputs the angular rates in those three orthogonal axes directly.

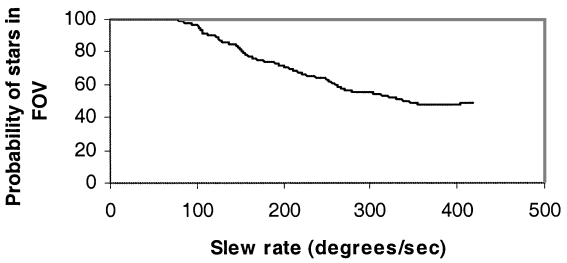

Fig. 9 Probability of having at least one detectable star in the FOV.

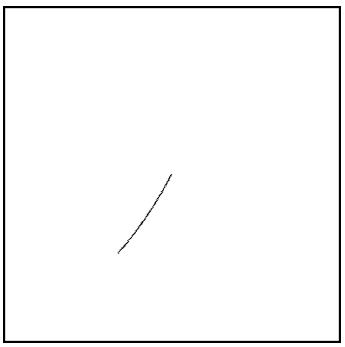

Fig. 10 Simulated stellar gyroscope image of a star streak. The image is shown negative.

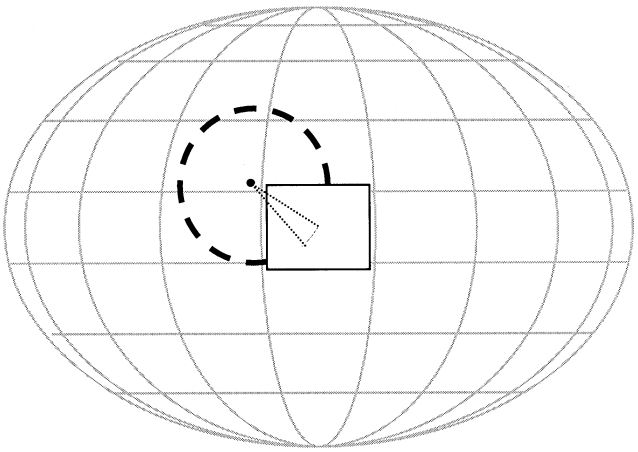

Fig. 11 Spin axis and spin angle are derived from the stellar gyroscope image.

Euler's theorem[21] states that any finite rotation of a rigid body can be expressed as a rotation through some angle about some fixed axis. This is utilized by the stellar gyroscope, which determines the spin angle Φ and the spin axis e. The spin rate and spin axis can then be transformed into rotations in three orthogonal axes, similar to the output from a conventional gyroscope using standard quaternion algebra.[21] A graphical illustration of how the stellar gyroscope operates is sketched in Figs. 10 and 11. Figure 10 shows a simulated stellar gyroscope image of a single star acquired at a high slew rate. In Fig. 11, the camera image is projected out on a unit sphere with the boresight pointing toward the reader. A spherical circle is then fitted to the star streak. The center of the spherical circle is the location of the spin axis relative to the boresight. Figure 11 also shows how the spin angle Φ can be determined.

When the stellar gyroscope is powered on, no knowledge about the spin rate exists. Therefore, it is unknown whether the stellar gyroscope should try to detect small bright spots or long dim star streaks. This has been solved by using a number of different filters that are optimized for detecting areas of different size. Initially, a simulation has been done to determine the maximum number of connected adjacent pixels in a binarized noisy image. (A binarized image is an image where all pixel values above a given threshold are set to 1 and all pixel values below the threshold value are set to 0.) The simulation used $\sim$1000 images for each threshold value, and the result is shown in Fig. 12. The simulations show that if a noisy image is binarized at, for example, 1.5σ, no areas with an area of larger than 13 pixels should be expected because of the noise.

Figure 13 shows an example of a simulated star image. This image is first binarized at 1σ, and all areas larger than 40 pixels (from Fig. 12) are detected. The image is then binarized at 1.1σ, and all areas with an area larger than 26 pixels (from Fig. 12) are detected. This is continued in steps of 0.1σ for all thresholds up to 3σ. Pixels located one pixel away from the bright center of the star streak also contain information. However, it is unlikely that they will be detected with this detection algorithm. Therefore the binarized image is dilated one iteration.[22] The resulting image is shown in Fig. 14.

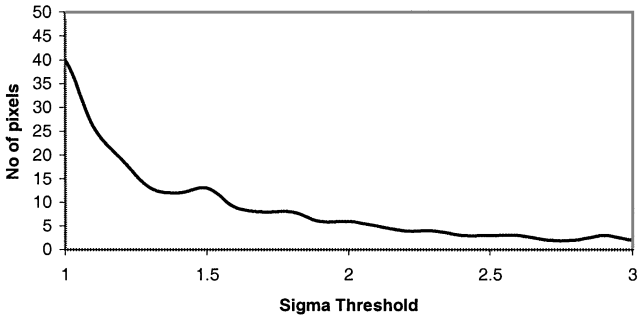

Fig. 12 Maximum number of adjacent pixels in a binarized noisy image.

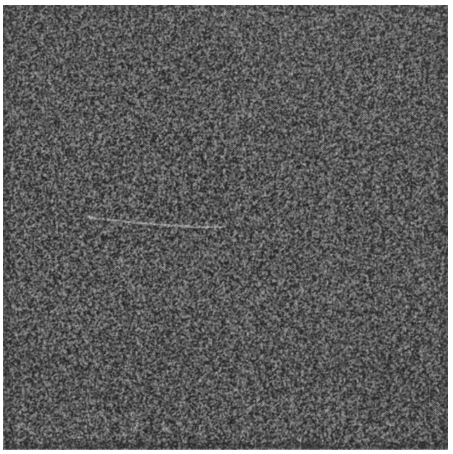

Fig. 13 Stellar gyroscope image. The spin axis is 65 deg away (directly north) from the boresight. The slew rate is 400 deg/s, and the star is M_V 0.

Fig. 14 Image from Fig. 13 has been binarized at multiple levels, and large areas have been identified. The image has been dilated one iteration.

It is observed in Fig. 14 that the star streak is broken up into six different areas because of the nature of the detection algorithm. It is not feasible to include all areas because some areas could be caused by noise or the image might contain star streaks from different stars. Therefore, the spherical circle fit procedure (described next) is invoked with all possible combinations of areas. More specifically, first the data from area 6 and no data from areas 1, 2, 3, 4, and 5 are sent to the spherical circle fitting routine. The quality of the fit (the residual between the perfect spherical circle and the actual data) is reported back. When the spherical fit routine has been evaluating all possible combinations (in this example $2^6 - 1 = 63$), the combination of areas that results in the smallest residuals are clustered together as belonging to the same star. Suppose that two clusters

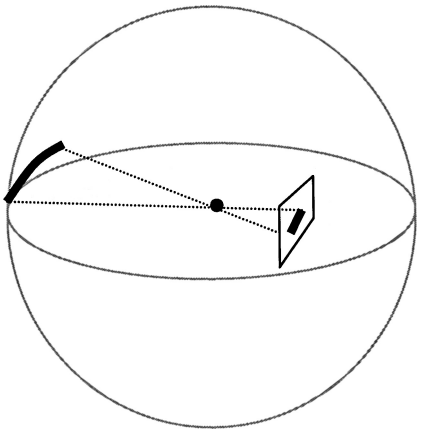

Fig. 15 Image on the focal plane is projected out on a unit sphere. The square inside the unit sphere is the focal plane.

of star areas are found with a low residual. Then the image spin axis/rate is found for both stars and the spin axis/rates are averaged.

Processing all possible combinations of areas is computationally intensive. It is possible to optimize this step of the algorithm either by combining areas one at a time or by simply assuming that all areas belong to the same star and removing them one at a time. However, the purpose of this paper has *not* been to optimize the algorithms, but only to show the feasibility.

The next step of the algorithm is to fit a spherical circle to the star streak. The assumption when fitting a spherical circle is that the spin axis of the spacecraft is constant. This is a reasonable assumption for the short period of the exposure time. Should it be an unreasonable assumption in a special spacecraft configuration/environment, the pixel data will have to be fitted to a more complex mathematical model.

Initially, the camera image is projected out on a unit sphere. For details, see Ref. 12. This is sketched in Fig. 15.

At this point the star streak consists of N points (pixels) on a unit sphere with an associated brightness. In other words, we have four vectors:

$$\begin{pmatrix} x_1 \\ x_2 \\ \cdots \\ x_N \end{pmatrix} \begin{pmatrix} y_1 \\ y_2 \\ \cdots \\ y_N \end{pmatrix} \begin{pmatrix} z_1 \\ z_2 \\ \cdots \\ z_N \end{pmatrix} \begin{pmatrix} b_1 \\ b_2 \\ \cdots \\ b_N \end{pmatrix} \tag{3}$$

where x_i, y_i, and z_i are the Cartesian coordinates of the pixel line of sight and b_i is the associated pixel brightness. We now want to find the best center of a spherical circle on which the points lie. The azimuth angle α and elevation angle δ of the center of the spherical circle can be converted into Cartesian coordinates with the usual equations[12]:

$$x_c = \sin\delta \cdot \cos\alpha \qquad y_c = \sin\delta \cdot \sin\alpha \qquad z_c = \cos\delta \tag{4}$$

The angular distance between a given point i and the center of the spherical circle is then

$$\phi_i = a\cos(x_c \cdot x_i + y_c \cdot y_i + z_c \cdot z_i) \tag{5}$$

A spherical circle is characterized by a constant angle from the center point to all points on the circumference. Therefore, for a given (α, δ) the angular distance to all points are calculated. A perfect circle fit would be characterized by a constant ϕ for all points. In other words, the standard deviation of the ϕ is 0. Each point has brightness b_i associated with it. Because the brightest pixels lie at the center of a star streak, these should have more weight than dim pixels, which are more likely to include noise. Therefore, the brightness of the pixels is also used in calculating the standard deviation, where the weight is proportional to its brightness. It is now possible to make

a cost function for finding the center of the spherical circle.

$$\text{cost} = \sqrt{\frac{wN \cdot wa2 - wa^2}{wN \cdot (wN - 1)}} \tag{6}$$

where

$$wN = \sum_{i=1}^{N} b_i, \quad wa = \sum_{i=1}^{N} b_i \cdot \phi_i, \quad wa2 = \sum_{i=1}^{N} b_i \cdot \phi_i \cdot \phi_i \tag{7}$$

It is simple to find the set of (α, δ) that will result in the minimum cost function using MATLAB's fminsearch function, which utilizes the Nelder–Mead Simplex algorithm for gradient descent search, or the Microsoft Excel solver function. The solution is the center of the spherical circle that best fits the data. In a real implementation of the algorithms, it would not be acceptable to utilize the Nelder–Mead simplex algorithm due to processing power considerations, and an analytical solution would have to be derived.

With the spin axis determined, it is not difficult to also determine the spin angle Φ of the stellar gyroscope. The spin angle of the stellar gyroscope is determined as an angle in a spherical triangle. The three corner points in the spherical triangle are the spin axis itself and both ends of the star streak. The two endpoints on the star streak are identified utilizing the original binarized star image.

The equation for calculating the spherical angle is ($\Phi = A$):

$$A = a\cos\left(\frac{\cos a - \cos b \cdot \cos c}{\sin b \cdot \sin c}\right) \tag{8}$$

where a is the angular distance between the two endpoints of the star streak, b is the angular distance between one endpoint on the star streak and the spin axis, and c is the angular distance between the other endpoint on the star streak and the spin axis.

It is difficult to accurately determine the center of a circle if only a small portion of the arc is visible. This would occur at low slew rates and at short exposure times. It is therefore imperative that the stellar gyroscope has a variable exposure time to adjust the spin angle of the star streaks. The stellar gyroscope will therefore autonomously adjust its exposure time so that a large spin angle is visible. On the other hand, both the start and the end of the star streak must be in the FOV; otherwise, it is not possible to determine the spin angle. Because the FOV is 56 deg, it was decided that a reasonable spin angle would be 30 deg. In relative attitude mode, the stellar gyroscope therefore continuously adjusts the exposure time so the spin angle is always close to 30 deg.

The stellar gyroscope will only operate in relative attitude mode at slew rates over 50 deg/s. (At lower rates it will operate in absolute attitude determination mode.) According to Fig. 6, only stars brighter than M_V 2.5 will be detected at this slew rate. Therefore, simulations of the stellar gyroscope have been performed for M_V 0 and 1 stars. In the first simulation, shown in Fig. 16, the accuracy of the spin axis has been simulated as a function of the angular distance between the boresight and the spin axis. The simulation has been performed at four spin rates (exposure times): 50 deg/s (600 ms), 100 deg/s (300 ms), 200 deg/s (150 ms), and 400 deg/s (75 ms). It is observed that the spin axis can always be determined to an accuracy of ~1 deg for a bright M_V 0 star. It is also observed that the error of the spin axis estimate increases significantly with a M_V 1 star when the angle between the boresight and the spin axis is larger than 40 deg. This is because the S/N ratio becomes very low, making it difficult to correctly fit a spherical circle to the star streak. More precisely, a few of the solutions are completely wrong (false positives), and these solutions impact the statistics. This does not mean that the stellar gyroscope does not work on M_V 1 stars or that it is inaccurate. But a number of estimates of the spacecraft spin axis must be made. These estimates must be consistent, and the bad estimates should be discarded.

In Fig. 17 the accuracy of the spin angle Φ is simulated as a function of the distance between the spin axis and the boresight.

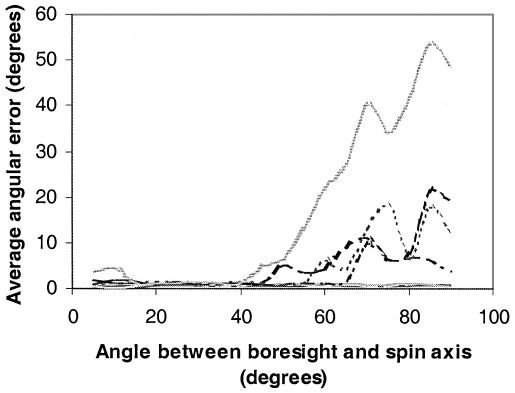

Fig. 16 Accuracy of the spin axis as a function of the angle to the spin axis: ——, mag 0, 50 deg/s; ——, mag 0, 100 deg/s; – – –, mag 0, 200 deg/s; ——, mag 0, 400 deg/s; – – –, mag 1, 50 deg/s; – – –, mag 1, 100 deg/s; - - -, mag 1, 200 deg/s; and ——, mag 1, 400 deg/s.

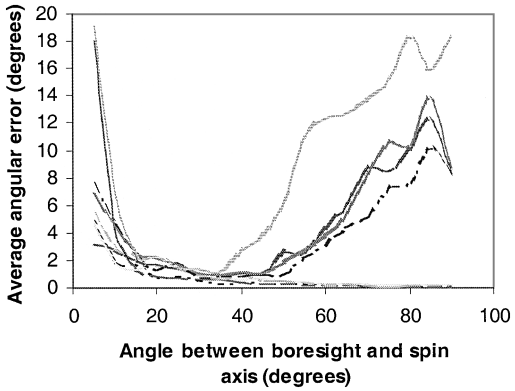

Fig. 17 Accuracy of the spin angle as a function of the angle between the boresight and the spin axis: - - - -, mag 0, 50 deg/s; – – –, mag 0, 100 deg/s; ——, mag 0, 200 deg/s; – – –, mag 0, 400 deg/s; – - - -, mag 1, 50 deg/s; ——, mag 1, 100 deg/s; ——, mag 1, 200 deg/s; and ——, mag 1, 400 deg/s.

As with the simulation shown in Fig. 16, four spin rates (exposure times) were used: 50 deg/s (600 ms), 100 deg/s (300 ms), 200 deg/s (150 ms), and 400 deg/s (75 ms) and for M_V 0 and 1 stars. Because of the geometry, it is not possible to determine the spin angle when the spin axis is very close to star.

As an example, consider the bright star in the center of the image in Fig. 4. It is difficult to fit a circle to this bright, short star streak. It is observed in the simulation that it is often possible to determine the spin angle of an M_V 0 star to an accuracy of ~2 deg. With a dimmer star, the uncertainty of the spin angle increases. This is an artifact of the simulation in Fig. 16. When an inaccurate spin axis estimate has been adopted, it will also result in an inaccurate spin angle estimate. As in the case of the spin axis, the spacecraft can log a number of spin-angle estimates. The estimates that are consistent can then be used to discard the false positive estimates and get an accurate spin angle.

Stellar Gyroscope Accuracy in Relative Attitude Determination Mode

It has been shown that it is possible to determine the accuracy of the spin axis to better than 1 deg and to determine the spin angle to better than 2 deg in most cases for a bright star. It was also explained that the exposure time was adjusted to make the spin angle approximately 30 deg. This means that the error of the spin angle is approximately 2 deg/30 deg = 6.6%. The time is known to very high accuracy, and this means that the error on the angular rate is also ~6.6%. The total angular rate around the spin axis can be redistributed to the X, Y, and Z axes defined on the stellar gyroscope. On average, the error in each axis will be 6.6%/sqrt(3) = 3.8%. The spin axis uncertainty can also cause some spill over from one axis to another, that is, if the rotation axis is aligned perfectly with the

Table 2 Operational modes for the stellar gyroscope

Operational Mode	Update rate, Hz	Slew rate, deg/s	Sky coverage, %	Accuracy	Type of output
Three-axis-stabilized mode	198	~0	100	55 arcsec	Absolute three-axis attitude
Absolute star tracking mode	198	~0–50	100	~0.09 deg	Absolute three-axis attitude
High slew rate operation	~1	~50–420	50–100	5% of the rate	Spin rate and spin axis, but not polarity of spin

X axis but the spin axis is estimated (because of the uncertainty) to be 1 deg toward the Y axis. Then $\sin(1\text{ deg}) = 1.7\%$ of the X-axis rotational rate is transferred to the Y axis. The combined error of the stellar gyroscope is estimated to be less than 5% of the rate (each axis).

Stellar Gyroscope Update Rate in Relative Attitude Determination Mode

In the relative attitude determination mode, no a priori knowledge exists about the orientation, spin rate, or spin axis. Therefore, the entire image must be read out at each update. The APS chip consists of 356×356 pixels that can be read at a rate of 10 MHz. This means that the image read time is only 12 ms. However, in order to get a reasonable length star streak, it is probably necessary to expose the image for 75–600 ms. The processing described in this section is also very time consuming, with multiple threshold segmentations and cost function minimization. However, dedicated hardware or more effective algorithms could speed up the processing significantly. In conclusion, an update rate of 1 Hz seems realistic. This is very different from a gyroscope that will provide the slew rates at an update rate of ~100 Hz. The ADCS subsystem would have to be designed specially to operate in this mode.

Conclusions

This paper proposes a new instrument for spacecraft attitude determination—the stellar gyroscope. A stellar gyroscope is basically a star tracker that is capable of very fast update rates and capable of operating at very high slew rates. It would be able to provide the same type of information as a conventional star tracker and a conventional inertial gyroscope when it is able to see stars. At high slew rates it would only be able to calculate attitude at an update rate of ~1 Hz. The stellar gyroscope would not be able to determine the sun direction like a sun sensor, but would be able to determine if the sun was in the FOV.

The stellar gyroscope has a very wide FOV (56 deg). This means that if the Earth/moon/sun is inside this FOV, the stellar gyroscope will not operate. Stray light from the moon, the sun, and the Earth will have to be dealt with though careful use of baffles. At high slew rates the signals are very weak, and even small amounts of stray light will interfere with the operation of the stellar gyroscope. There could be scenarios of spacecraft motion where the stellar gyroscope consistently captured the sun/moon/Earth (or stray light from these bodies) in the FOV and did not operate at all. On the other hand, mounting two or more stellar gyroscopes pointing in different directions could mitigate this problem. In this way at least one stellar gyroscope would still work if the other(s) were disabled.

The advantage of using a stellar gyroscope compared to a conventional attitude determination system should be stressed. Because the technology of a stellar gyroscope is similar to a star tracker, it is likely that the cost, reliability, mass, and power will be similar to the state of the art in star trackers. However, the potential elimination of conventional gyroscopes will offer a significant improvement in power, mass, reliability, and cost for attitude determination systems.

The stellar gyroscope would operate in two modes. At low slew rates, or in three-axis stabilized mode, the stellar gyroscope would calculate absolute attitude like a conventional star tracker with very high update rates. At high slew rates, the stellar gyroscope would detect a star streak and determine the spin rate and spin axis of the instrument. The operational modes of the stellar gyroscope are summarized in Table 2.

An ADCS based on a stellar gyroscope would have to be designed very differently from a conventional system. The difference is primarily in detumbling and operation at high spin rates, where an attitude rate estimate is only available once a second. The polarity of the spin would not be known based on a single measurement from the stellar gyroscope either. One way to determine the polarity of the spin would be to take a long integration (to determine the spin axis and rate) followed by a short integration (to determine the spin polarity). The software complexity and requirements of the ADCS would be larger compared to conventional ADCS systems. However, the computational requirements of the stellar gyroscope are not prohibitive for a modern spacecraft computer. The stellar gyroscope allows an order-of-magnitude reduction in ADCS mass and power in comparison to present-day systems. This reduction trend will be essential to future miniature spacecraft.

Acknowledgments

The research described in this paper was carried out at the Jet Propulsion Laboratory, California Institute of Technology under a contract with NASA. The authors of this paper thank David S. Bayard and William G. Breckenridge, both of Jet Propulsion Laboratory, for reviewing this paper and providing valuable suggestions for improvement. The authors also thank five anonymous reviewers for reviewing this paper. References herein to any specific commercial product, process, or service by trademark, manufacturer, or otherwise, does not constitute or imply its endorsement by the United States Government or the Jet Propulsion Laboratory, California Institute of Technology.

References

[1]Thomas, V. C., Alexander, J. W., Dennison, E. W., Waddell, P., Borghi, G., and Procopio, D., "Cassini Star Tracking and Identification Architecture," *SPIE Proceedings*, Vol. 2221, Society of Photo-Optical Instrumentation Engineers, Bellingham, WA, 1994, pp. 15–26.

[2]Jørgensen, J. L., and Liebe, C. C., "The Advanced Stellar Compass, Development and Operations," *Acta Astronautica*, Vol. 39, No. 9–12, 1996, pp. 775–783.

[3]von Bezooijen, R. W. H., "True Sky Demonstration of an Autonomous Star Tracker," *SPIE Proceedings*, Vol. 2221, Society of Photo-Optical Instrumentation Engineers, Bellingham, WA, 1994, pp. 156–169.

[4]Cassidy, L. W., "Space Qualification of HDOS' HD-1003 Star Tracker, Space Sciencecraft Control and Tracking in the New Millennium," *SPIE Proceedings*, Vol. 2810, Society of Photo-Optical Instrumentation Engineers, Bellingham, WA, 1996, pp. 213–220.

[5]Pissavin, P., Krebs, J. P., Lelong, P., Vidal, P., and Navoni, R., "Improved Star Tracker for Odin Satellite," *ESA International Conference on Spacecraft Guidance, Navigation and Control Systems, Proceedings*, ESA, Noordwijk, The Netherlands, 1997, pp. 611–616.

[6]Paulsen, T. E., and Maresi, L., "Calibration and Verification of the TERMA Star Tracker for the NEMO Satellite," AIAA Paper 2000-5338, Sept. 2000.

[7]Wertz, J. R., *Space Mission Analysis and Design*, 3rd ed, Microcosm, Inc., Columbia, MD, 1992.

[8]Brady, T., Tillier, C., Brown, R., Jimenez, A., and Kourepenis, "The Inertial Stellar Compass: A New Direction in Spacecraft Attitude Determination," 16th Annual USU Conference on Small Satellites, Paper SSC 02-II-1, Utah State Univ., Logan, UT, Aug. 2002.

[9]Liebe, C. C., "Star Trackers for Attitude Determination," *IEEE AES Magazine*, June 1995, pp. 10–16.

[10]Lelong, P., Saint Pé, O., Vignon, B., Davancens, R., Farré, J., Magnan, P., and Duverger, T., "Miniature GNC Sensors Using APS Devices," *Proceedings of 4th ESA International Conference on Spacecraft Guidance, Navigation and Control Systems*, ESTEC, Noordwijk, The Netherlands, 2000, pp. 273–278.

[11]Pain, B., Yang, G., Ortiz, M., McCarty, K., Hancock, B., Heynssens, J., Cunningham, T., Wrigley, C., and Ho, C., "A Single-Chip Programmable Digital CMOS Imager with Enhanced Low-Light Detection Capability," *Proceedings of the 13th VLSI Design Conference*, IEEE Press, New York, 2000, pp. 342–347.

[12]Liebe, C. C., "Accuracy Performance of Star Trackers—A Tutorial," *IEEE Transactions on Aerospace and Electronics Systems*, Vol. 38, No. 2, 2002, pp. 587–599.

[13]Liebe, C. C., Alkalai, L., Domingo, G., Hancock, B., Hunter, D., Mellstrom, J., Ruiz, J., Sepulveda, C., and Pain, B., "Micro APS Based Star Tracker (MAST)," *Proceedings of the 2002 IEEE Aerospace Conference*, Inst. of Electrical and Electronics Engineers, Piscataway, NJ, 2002, pp. 2285–2299.

[14]van den Heide, E. J., Kruijff, M., Douma, S. R., and Lansink, D. O., "Development and Validation of a Fast and Reliable Star Sensor Algorithm with Reduced Data Base," International Astronautical Federation, IAF Paper 98-A605, Paris, France, Sept.–Oct. 1998.

[15]Liebe, C. C., "Pattern Recognition of Star Constellations for Spacecraft Applications," *IEEE Aerospace and Electronic Systems Magazine*, Vol. 7, No. 6, 1992, pp. 34–41.

[16]Padgett, C., Kreutz-Delgado, K., and Udomkesmalee, S., "Evaluation of Star Identification Techniques," *Journal of Guidance, Control, and Dynamics*, Vol. 20, No. 2, 1997, pp. 259–267.

[17]Udomkesmalee, S., Alexander, J. W., Tolivar, A. F., "Stochastic Star Identification," *Journal of Guidance, Control, and Dynamics*, Vol. 17, No. 6, 1994, pp. 1283–1286.

[18]Mortari, D., "Search-Less Algorithm for Star Pattern Recognition," *Journal of Astronaut Sciences*, Vol. 45, No. 2, 1997, pp. 179–194.

[19]Liebe, C. C., Dennison, E. W., Hancock, B., Stirbl, R. C., and Pain, B., "Active Pixel Sensor (APS) Based Star Tracker," *Proceedings of the Institute of Electrical and Electronics Engineers Aerospace Conference*, Inst. of Electrical and Electronics Engineers, Piscataway, NJ, 1998, pp. 119–127.

[20]Hancock, B. R., Stirbl, R. C., Cunningham, T. J., Pain, B., Wrigley, C. I., and Ringold, P. G., "CMOS Active Pixel Sensor Specific Performance Effects on Star Tracker/Imager Position Accuracy," *Proceedings of the Society of Photo-Optical Instrumentation Engineers*, Vol. 4284, Society of Photo-Optical Instrumentation Engineers, Bellingham, WA, 2001, pp. 43–53.

[21]Wertz, J. R., *Spacecraft Attitude Determination and Control*, Kluwer Academic, Norwell, MA, 1990, pp. 761, 762.

[22]Gonzalez, R. C., and Woods, R. E., *Digital Image Processing*, Addison Wesley Longman, Reading, MA.